International Journal of Material Forming (2022) 15: 24
https://doi.org/10.1007/s12289-022-01670-y

ESAFORM 25 YEARS ON

Changes in processing characteristics and microstructural evolution during friction extrusion of aluminum

Ricardo M. Halak[1] · Lars Rath[1] · Uceu F. H. R. Suhuddin[1] · Jorge F. dos Santos[1] · Benjamin Klusemann[1,2]

Received: 18 November 2021 / Accepted: 16 February 2022 / Published online: 12 March 2022

Abstract

This study focuses on characterizing the microstructural evolution of the aluminum alloy 7075 in the friction extrusion process under different extrusion forces and die angles. Depending on these conditions, two fundamentally different extrusion types are found, showing significant differences in the process characteristics and microstructural evolution. One of the two extrusion types is associated with high extrusion force and low die angle, leading to fully recrystallized wires with average grain size around 1.2 µm. The microstructural analysis indicates that the microstructure present in the wires is generated in the charge material by the combination of tool geometry, load induced material flow and friction conditions in the initial stages of the friction extrusion process. The identified processing conditions and influencing factors introduce an alternative route for friction extrusion at low extrusion ratios, capable of producing completely refined wires.

Keywords Friction extrusion · Aluminum alloy · Dynamic recrystallization · Solid state processing · Mechanical properties · Ultra-fine grains

Introduction

The industrial development fostered the enhancement of processing techniques able to improve materials properties, allowing manufacturing of products that present tailored property combinations, such as high strength, high ductility and superplasticity at low temperatures [1, 2]. Aluminum alloys play a significant role in this market due to their outstanding combination of properties, such as strength, toughness, density, and corrosion resistance [3]. Among the numerous techniques used in aluminum processing and its alloys, friction based processes, such as friction stir welding/processing (FSW/P), have gained prominence over the last years, becoming widely used in industry [4–7]. Localized heat input limited to the stir zone, potential cost reduction due to lower energy requirements, and improvement in mechanical properties, such as strength, ductility and fatigue behavior, are just some of the advantages of FSW/P [8, 9]. Recently, friction extrusion (FE) has received significant attention for its capability to shape different materials into fully consolidated extrudates (rods and wires) while providing excellent combinations of mechanical properties, such as high elongation at break and high tensile strength related to the microstructural refinement of the processed material [10, 11].

Based on the same principles as FSW/P [12], FE is characterized as solid state process involving severe plastic deformation and frictional heating to produce extrudates from metallic charge materials [13]. Using a non-consumable, rotating die that is pressed against the charge material, the extrusion takes place by friction and heat generation at the die-charge interface. The charge material can be in various conditions, such as chips, powder or bulk material [13]. The friction at the die-charge interface introduces severe plastic deformation and generates heat that softens

✉ Ricardo M. Halak
ricardo.halak@hereon.de

✉ Lars Rath
lars.rath@hereon.de

Uceu F. H. R. Suhuddin
uceu.suhuddin@hereon.de

Jorge F. dos Santos
jorge.dos.santos@hereon.de

Benjamin Klusemann
benjamin.klusemann@hereon.de

[1] Solid State Materials Processing, Institute of Materials Mechanics, Helmholtz-Zentrum Hereon, Max-Planck-Str. 1, 21502 Geesthacht, Germany

[2] Institute of Product and Process Innovation, Leuphana University of Lüneburg, Universitätsallee 1, 21335 Lüneburg, Germany

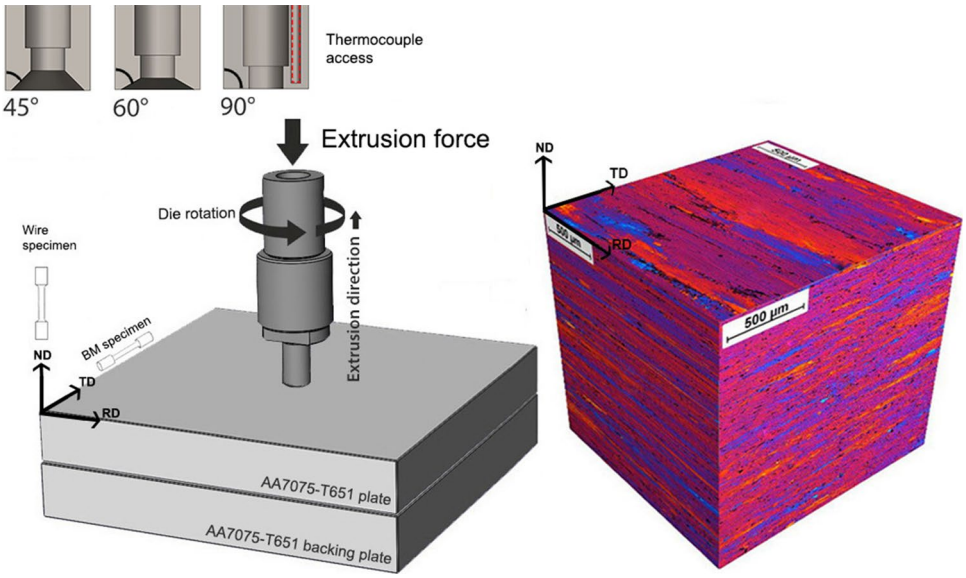

Fig. 1 FE set-up and die angles used. The position of the thermocouple is illustrated in the 90° die angle. The initial microstructure of the AA7075-T651 charge material is shown on the right, i.e. rolling (RD), transverse (TD), and normal direction (ND) and the orientation of the extracted samples for mechanical testing is sketched

the charge material, which then is pressed through the die, forming wires or rods [14]. The combination of severe plastic deformation and elevated temperature induces dynamic recrystallization, resulting in microstructural refinement [15]. In comparison to conventional extrusion, FE is a one-step process that can use lower extrusion forces due to the localized heat introduction via friction, saving time and energy by eliminating the necessity for preheating [16]. Since the processing takes place in solid state, the reactions and phase transformations commonly involved in casting and solidification are avoided, preventing undesirable defects, such as shrinkage, gas porosity or segregation [17–19].

Efforts have been made to understand and determine the effects of process parameters, such as rotational speed and die angle on the extrudates [10, 11, 20]. Ansari et al. [10] fabricated fully consolidated and defect-free wires from magnesium chips, showing rotational speed as a critical parameter to the soundness of the wires. The magnesium wires exhibited higher strength and elongation than the base material as a consequence of the microstructural refinement. Tang et al. [11] extruded wires from AA2050 and AA2195 chips via FE, obtaining fully recrystallized microstructures with equiaxed grains. Behnagh et al. [21] produced defect-free wires from AA7277 machining chips at constant die movement, where high values of rotational speed led to the formation of hot cracks, while low rotational speeds resulted in cold tear.

In this work the 7075 aluminum alloy is employed, which is commonly used for aircraft and aerospace structural applications due to its good strength to density ratio, fracture toughness and corrosion resistance [22, 23]. Since AA7075 shows a limited processability, it facilitates to identify indications of either too hot or too cold extrusions and to establish a clear classification of a suitable processing parameter window, related to the inherent low ductility and incipient melt behavior [22–24]. Additionally, the potential improvement in processing costs and extrudate properties makes this alloy a suitable candidate for FE as recently shown by Whalen et al. [25]. AA7075 has zinc as primary alloying element and additions of magnesium and copper, which enable this alloy to be heat treatable. Consequently, the mechanical strength is strongly dependent on precipitation hardening [26].

Despite the contributions made by studies regarding the consolidation by FE of several materials from different states (powder, chips, bulk) and the feasibility of producing defect-free extrudates (wires and rods), the effects of individual extrusion parameters on the material flow as well as the friction mechanisms still remain partially unclear. Furthermore, it is still necessary to elucidate the processing conditions in FE and define correlations that enable a more effective control of the resulting microstructure and properties of the extrudates. Addressing this knowledge gap, the objective of the present work is to investigate the processing conditions during friction extrusion of AA7075-T651 with focus on fundamental correlations between control parameters and properties of the extruded wires, allowing the identification of critical conditions to the microstructural evolution during FE.

Experimental methods

The FE experiments were performed on a custom-designed friction surfacing system (RAS), manufactured by Henry Loitz Robotik (Germany), providing suitable process conditions to conduct friction extrusion from plate material. A sketch of the used FE set-up is illustrated in Fig. 1. It

Table 1 Chemical composition of the AA7075-T651 charge material, obtained by optical emission spectrometry (OES) performed by NUTECH GmbH (Neumünster, Germany) according to in-house procedure HV02:2019

Element	Al	Zn	Mg	Cu	Fe	Cr	Mn	Si
wt.%	Bal.	5.8	2.3	2.0	<0.3	<0.2	<0.2	<0.1

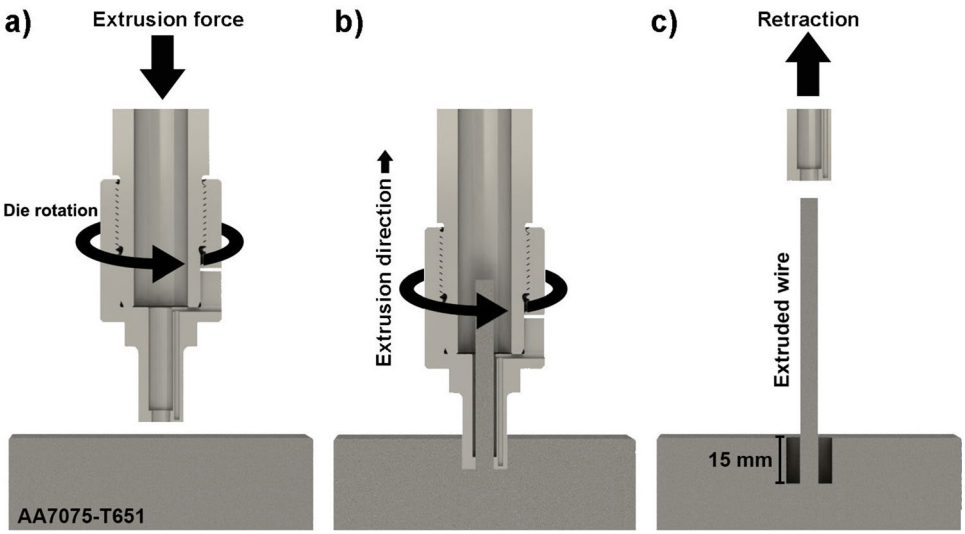

Fig. 2 Schematic of the processing steps during friction extrusion: a) The die rotates while an extrusion force is applied. b) The die advances into the charge material until a specified depth is reached. c) The rotating die is retracted and the wire is left connected to the plate

consists of an aluminum plate clamped on the working table of the machine and the die attached to the rotating spindle. Rolled AA7075-T651 plates (200 mm x 200 mm x 30 mm) were used as charge material, see chemical composition in Table 1. The T651 condition was chosen for scientific purposes to provide homogeneous properties throughout the feedstock material. Additionally, the high strength allows to minimize flash formation during FE from plate material. In order to guarantee a homogeneous heat transfer during the process, a backing plate of the same alloy and dimensions was used. During the experiments, both plates were held down on the working table of the RAS machine by clamping the stack at the four corners. Furthermore, the plates were preheated to 40°C to ensure identical starting conditions for each FE process.

The initial microstructure of the employed AA7075-T651 plates is shown in Fig. 1, characterized by long elongated grains, typical after rolling. The utilized extrusion die has an external diameter of 15 mm with the central extrusion channel featuring a diameter of 6 mm, which leads to an extrusion ratio (ER) of 6.25[1]. The use of the relatively low ER allows for better microstructural visualization and distinction of process affected zones. The extrusion dies were manufactured from AISI H13 steel. Three different die angles were investigated in this study, i.e. 90°, 60° and 45°, see Fig. 1. The rotational speed of the die during FE was set to 300 min^{-1}, while the extrusion force was varied between 16 kN and 22 kN. The thermal cycles during FE were determined for different extrusion forces on basis of the 90° die angle, utilizing a Conatex K-type thermocouple, recording the temperature at 1 Hz. The thermocouple was positioned 1 mm behind the die face, at 2/3 of the radius, ensuring mechanical contact with the die via spring tension, as indicated in Fig. 1 for the 90° die angle.

The different steps of the employed force-controlled FE process are illustrated in Fig. 2: a) The tool rotates at a constant rotational speed and the extrusion force is applied, resulting in the plasticization of the material located at the die-charge contact zone. b) During extrusion, the severely plasticized material is forced through the central channel of the die, leading to a wire shape. The process is stopped at 15 mm of die advance into the plate, i.e. half the thickness of the plate, resulting in a nominal wire length of 93.8 mm (for 90° die angle), 85.3 mm (60°), or 79.3 mm (45°). c) The rotating extrusion die is retracted and the wire is left connected to the plate.

In order to analyze the FE process and the resulting wires, the extruded wire including the charge material were cut, ground and polished for metallographic characterization. In terms of the longitudinal section of the wires, samples were taken and analyzed from positions between approximately 40 and 70 mm of the extruded wire length.

[1] Assuming no significant flash formation during plunging into the plate.

The metallographic preparation consisted in grinding until 4000# sandpaper, polishing with 1 µm diamond solution and electrochemical etching with Barker's Reagent. Optical analysis was performed with a VHX-6000 digital microscope, Keyence, Germany as well as a Leica DMi8, Leica Microsystems, Germany. Furthermore, the microstructure was analyzed by FEI Quanta 650 scanning electron microscope (SEM) equipped with a Velocity electron backscatter diffraction (EBSD) system. Orientation mapping involving automatic beam scanning was performed with a scan step size of 0.1 µm. A 15° criterion was employed as minimum misorientation angle to calculate the grain size.

Tensile tests were performed according to ISO 6892-1:2016. Tensile specimens with 4 mm diameter and 20 mm of gauge length were machined from the extruded wires. The specimens were extracted in such a way that the gauge length was located between 30 to 50 mm of the extruded wire length, having the tensile testing axis parallel to the extrusion direction as illustrated in Fig. 1. The tensile testing axis of the base material specimens was the transversal direction (TD). The tensile tests of the wires were performed at cross head speed of 0.3 mm/min using a Zwick universal testing machine after natural aging for more than 28 days, assuming no significant further precipitation evolution. The respective natural aging time, i.e. the time between extrusion and tensile testing, is reported for the individual wires in the following. Focusing only on the resulting material properties of the as-extruded wires, half the thickness of the plate, no further heat treatment procedure is applied. A Struers DuraScan G5 is employed to measure the hardness of the wires (0.2 HV) 65 days after extrusion. Similar to the tensile specimens, the hardness measurements were performed at 30 to 50 mm of the wire length.

Results and discussion

Typical microstructures after friction extrusion

As it is well accepted in the literature, the material in FE flows in a helical shape [13, 27]. In an attempt to visualize the metal flow pattern in FE of aluminum alloys, Li et al. [13, 28] conducted extrusions of AA6061 utilizing AA2195 as marker insert located at 1/3 of the radius of the AA6061 cylinders, showing that the marker material follows a spiral path, being gradually dragged into the center of the wire as the extrusion progresses. Similar spiral-like patterns were observed by Li et al. [29], extruding AA1010 and using AA2050 as marker material. This metal flow results from the combination of friction and severe plastic deformation imposed in FE and typically leads to the formation of different microstructure zones within the solid extruded wire. A typical resulting microstructure in the wire and the connected charge material for an applied extrusion force of 16 kN, a 90° die angle and a rotational speed of 300 min^{-1} is shown in Fig. 3. Refined and equiaxed grains are found within the thermo-mechanically affected zone (TMAZ) of the charge material as well as the outer diameter of the extruded wire (Region A). In the central portion of the wire, coarse and deformed elongated grains are encountered (Region C), resulting from charge material flowing towards the center of the forming wire. Therefore, this zone is typically called the material flow zone in conventional extrusion processes [30]. A transition zone is located between regions A and C with semi-recrystallized, coarse and elongated grains (Region B). EBSD analyses of the different regions reveal that Region A presents 86.5 % of high-angle grain boundaries, an average grain size of 1.3 µm with 97.9 % smaller than 3 µm and 43.3 % in the submicrometer range, see Fig. 4. In Region B, the fraction of high-angle grain boundaries decreased to 43.4 % while the fraction of low-angle grain boundaries increased to 33.9 %, both results indicate a less effective recrystallization in the Region B. Regarding grain size, 80 % of the Region B was constituted by 2 µm equiaxed grains, while the remaining grains exhibit mainly grain sizes between 5 and 70 µm.

The observed microstructural zones in the produced wires are in agreement with the literature of conventional extrusion [31], where different shear application between the periphery and the center of the charge material are reported to influence the final microstructure of the wire. For FE, similar microstructural patterns were found by Baffari et al. [32] for AA2050. Behnagh et al. [33] reported gradual reduction in grain size from the center of the wire toward its boundary in FE of magnesium chips. The findings made by Li et al. [13] and Baffari et al. [32] associated the formation of finer grains in the outer diameter of the wires with a higher level of deformation that the material closer to the wall of the extrusion channel undergoes in comparison to the center of the charge material. The observation that the fraction of high-angle grain boundaries encountered in Region A of the extruded wires is higher than in Region B, supports the hypothesis that Region B represents a transition between Region A and C associated to a progressive decrease in shear introduction from the outer diameter towards the center of the processing zone. With decreasing shearing, the lower resulting strain can no longer sufficiently induce recrystallization, resulting only in partial recrystallization in Region B [26, 34–38]. It should also be mentioned that low extrusion ratios, such as 6.25, reduce the extent of deformation applied to the billet, facilitating the formation of non-recrystallized regions in the center of the wire and resulting in the microstructural pattern observed.

Since the extrusions are performed using a plate set-up, Fig. 1, the effect of flash formation is illustrated in Fig. 3 as well. The micrograph presents the typical size and shape of the flash formed during FE on the top of the plate around

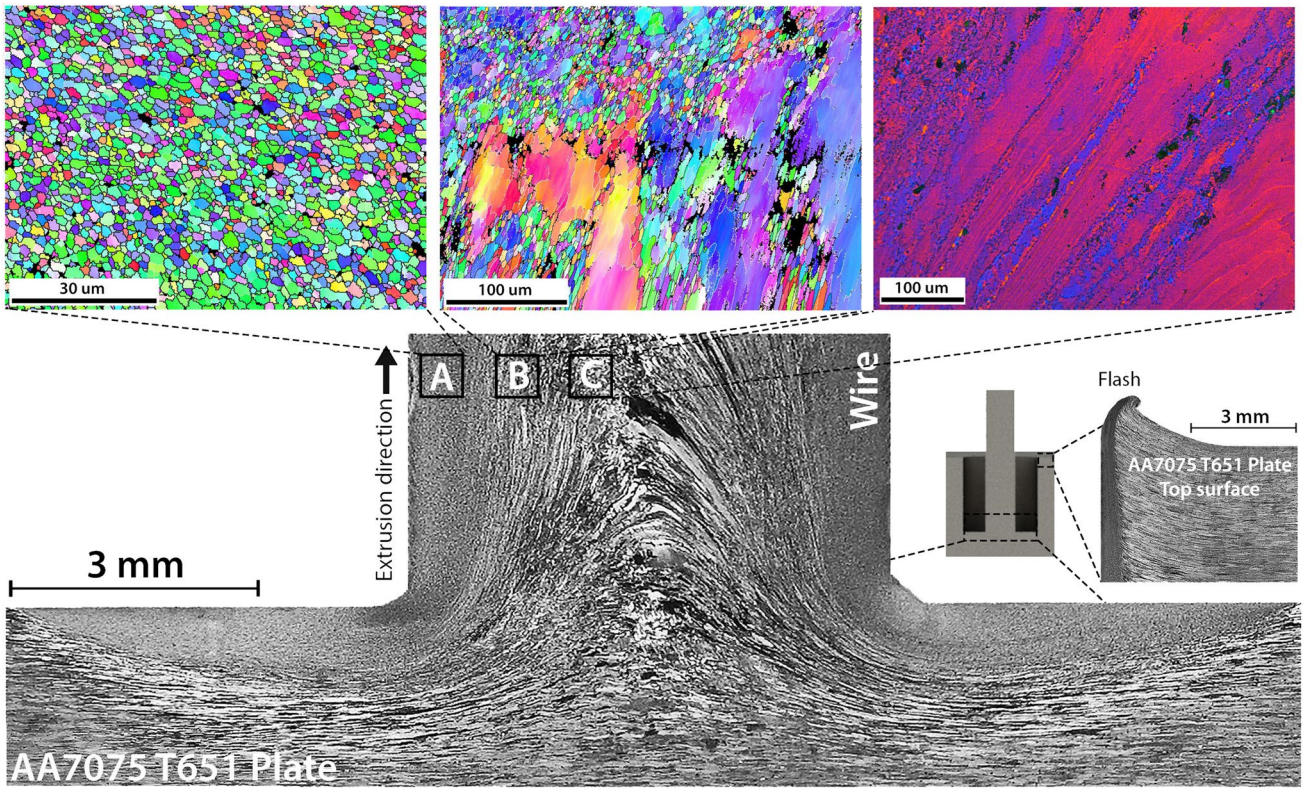

Fig. 3 Microstructural zones formed during FE at an extrusion force of 16 kN for 90° die angle at a rotational speed of 300 min^{-1}. Three different microstructural regions are identified within the wire (A-C). On the right, the typical flash formation at the top of the plate after FE is illustrated

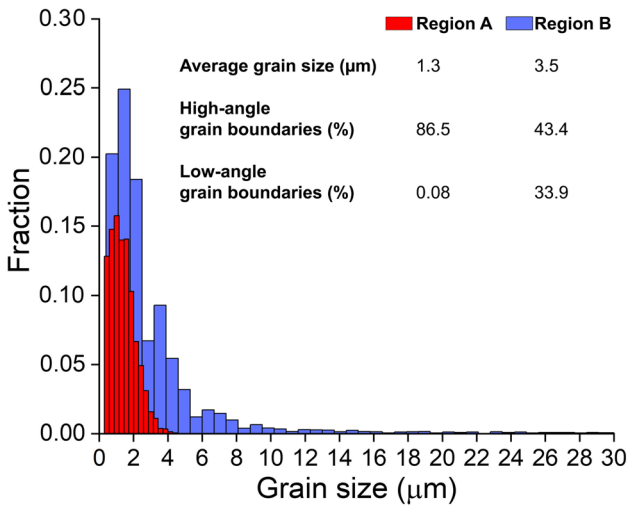

Fig. 4 Grain size distributions within Regions A and B obtained by EBSD analysis of the wire extruded with 16 kN extrusion force, 90° die angle and rotational speed of 300 min^{-1}

the die. The flash volume was estimated based on the micrographs, representing approximately 5.3% of the theoretical volume of the extruded wire, which is assumed negligible regarding the targeted extrusion ratio of 6.25.

In the following, the effect of an increase in extrusion force is analyzed for the 90° die angle. As illustrated in Fig. 5, increasing the extrusion force from 16 kN to 20 kN leads to widening of Region B towards the center. It can be noticed that the processing time is significantly reduced with increasing extrusion force, i.e. higher extrusion rates. As Fig. 6 shows, an extrusion force increase results in elevated extrusion temperatures, which enables higher extrusion rates. AA7075 shows a substantial decrease in tensile strength and increase in ductility, for temperatures above 200°C [39, 40], which has a significant effect on the resulting material flow behavior and extrusion resistance during FE. Based on the metal forming and metallurgy literature [26, 34–38], extrusions at higher extrusion rates caused by the application of higher extrusion forces at elevated extrusion temperatures, might lead to a progressive reduction of stored energy and shear application into the material, diminishing the recrystallized fractions since the dislocation density and crystalline defects are not sufficient to induce recrystallization. Consequently, higher extrusion forces present less effective recrystallization in FE for the 90° die angle.

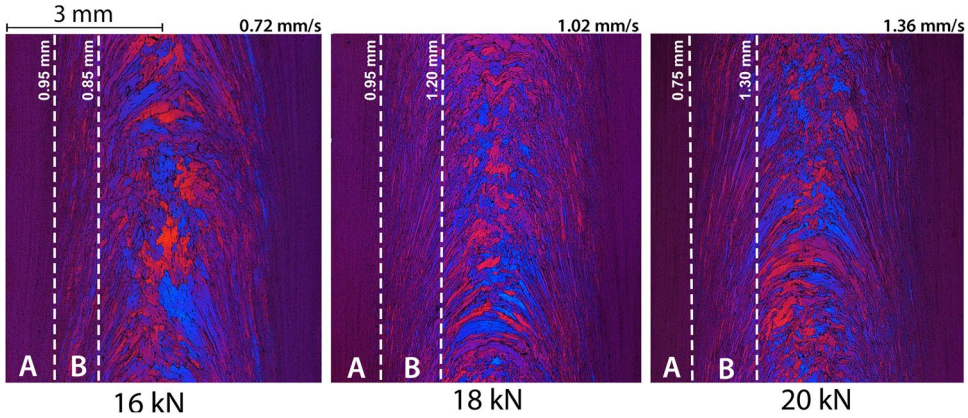

Fig. 5 Microstructures obtained at 16 kN, 18 kN and 20 kN extrusion force and corresponding average extrusion rate as well as width of regions A and B in wires extruded with 90° die angle at 300 min^{-1}

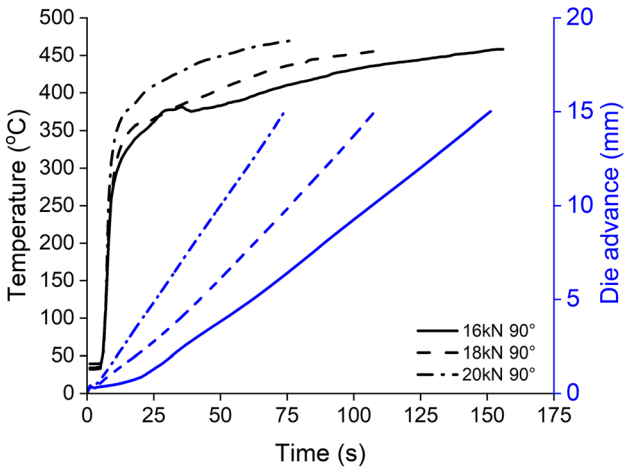

Fig. 6 Temperature and corresponding die advance, i.e. penetration into the charge material, for FE of AA7075 with the 90° die angle at 300 min^{-1} at different extrusion forces (16 kN, 18 kN, 20 kN)

The temperature measurements confirm observations made in previous studies of FE [11, 13], presenting analogies to results in FSW/P. Li et al. [13] stated that a continuous heat input takes place in FE with insufficient heat dissipation at constant process parameters, resulting in a continuous increase in temperature. Therefore, no steady-state in terms of temperature is reached, which is confirmed by the temperature results encountered, see Fig. 6. Overall, the measured maximum temperatures for the processes at different extrusion forces reached up to 469°C. Since the temperature was measured at a distance of 1 mm from the die face, the temperature of the extruded material may be even slightly higher. Considering that the solidus temperature of AA7075-T651 is 476°C [39, 40], local melting, i.e. incipient melting, may occur during the process at higher extrusion forces, however, within the micrographs no indication of this effect was observed. In addition, the heating rates are an important factor in friction processing methods of aluminum alloys, since high heating rates can lead to spontaneous melt of second phase particles, such as η, S and T in AA7075, by preventing dissolution before the respective melting temperature is reached [24]. For instance, for refill friction stir spot welding of AA7075 this effect was reported for heating rates in the range of 210 to 440 K/s [24]. Since the maximum heating rate in the current case of FE was determined to be 150 K/s, such spontaneous melting phenomena are not expected.

Finally, the influence of the die angle on the wire microstructure is analyzed for the low extrusion force of 16 kN. A decrease in die angle from 90° to 45° narrowed the Region A but showed a widening of Region B in the direction towards the center of the wire, see Fig. 7. This indicates that a decrease in die angle may be detrimental to the overall refinement of the wires, consistent with results reported by Yu et al. [41]. The reason is associated with the lower imposed deformation in the extruded material, originated by shorter time in which rotation affects the material[2] and smoother transition from the charge material into the wire for lower die angles. Since stored energy in form of crystalline defects introduced by deformation is one of the main driving forces for recrystallization, the smaller the imposed deformation, the less effective recrystallization [42]. In summary, the microstructure for the different die angles at the low extrusion force of 16 kN still shows similar characteristics as observed before for the 90° die angle.

Although the results so far indicate that a lower die angle and higher extrusion force might be detrimental for a very fine recrystallized microstructure, a transition in process behavior is observed for the 60° die angle during processing, which was not present for the 90° die angle. To reveal this, serial extrusions at different plunge depths were performed. A change in the shape of the affected region in the charge material was observed over time, as illustrated by the yellow dash line in Fig. 8. In the initial stages of extrusion, the affected profile has three concavities and the wire presents

[2] The decrease in die angle led to a substantial increase in extrusion rate, by a factor of 3 and 6 for the 60° and 45° die angle, respectively.

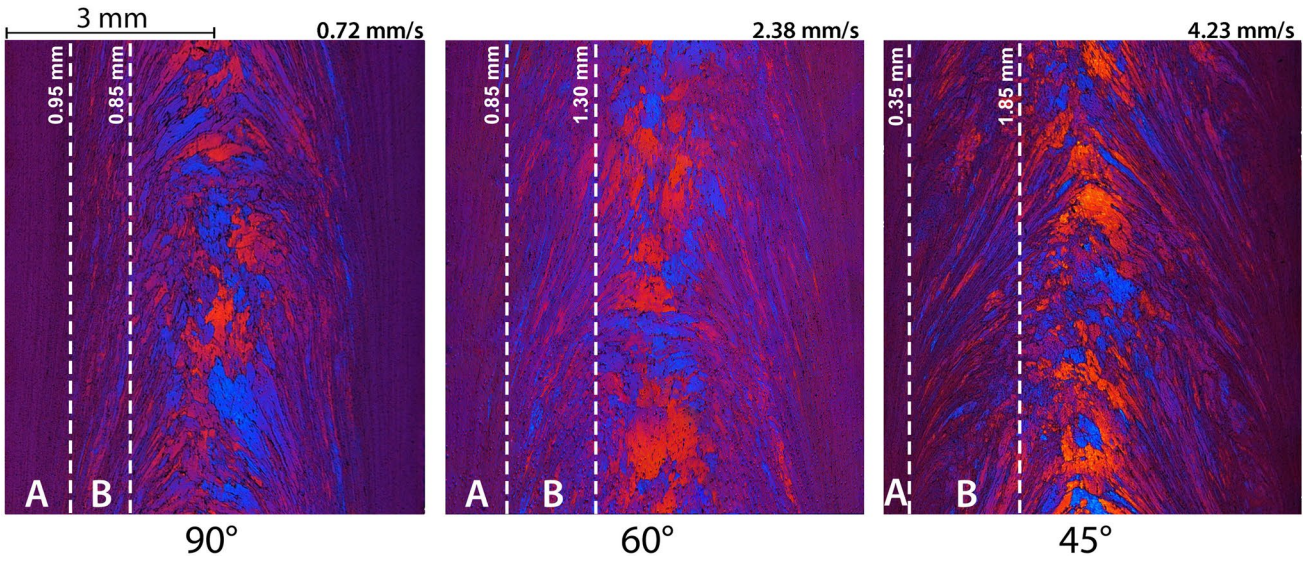

Fig. 7 Microstructure obtained with 90°, 60° and 45° die angle in wires extruded using 16 kN extrusion force at 300 min^{-1}, as well as corresponding average extrusion rate and width of regions A and B

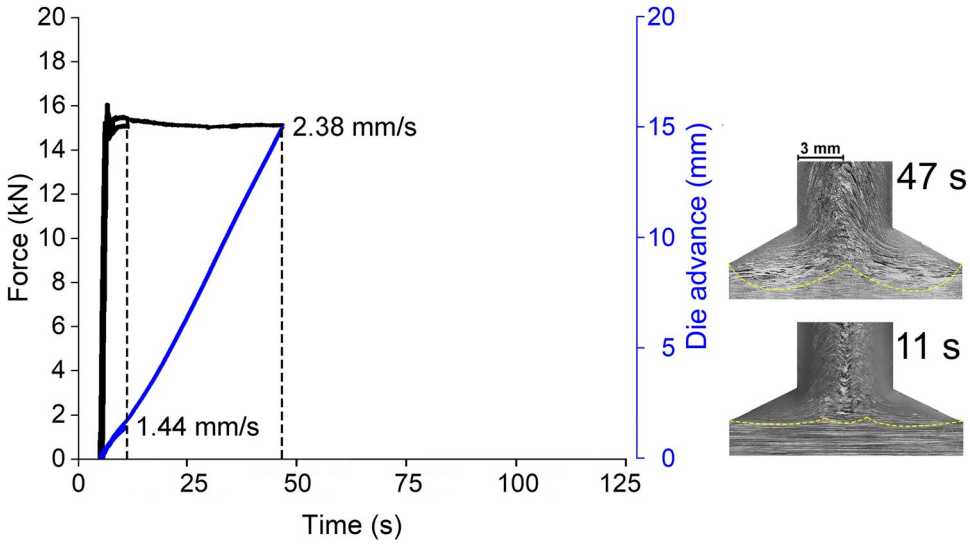

Fig. 8 Extrusion force, die advance and corresponding microstructure of wire and charge material over extrusion time using 60° die angle, 16 kN extrusion force at 300 min^{-1}. The transition in process behaviour leads to changes in microstructure and extrusion rate at different process times

a narrowed central zone and larger recrystallized fractions. Moreover, the material flow pattern inside the extruded wire follows the distribution observed in the charge material. This profile evolves as the extrusion continues and, although a larger region of the charge material is affected at 47 s, less recrystallization is observed in front of the die and in the wire, which is also correlated with a higher extrusion rate. The microstructure observed in the initial stage of extrusion shows a material flow that is similar to those already reported for conventional extrusion [31], which is associated with more severe shear deformation. Inhomogeneous charge material properties and non-uniform temperature distribution in the charge material are also conditions involved with the generation of this material flow [31]. On the other hand, similar patterns as the one formed at the end of the process are encountered in conventional extrusion under fully lubricated, low friction conditions [31].

Conditions for homogeneous microstructural refinement

Next to the observed transition within one FE process, as discussed in the previous section, fundamentally different process characteristics between FE processes performed at different extrusion forces and die angles were identified, as illustrated in Fig. 9. The two different process characteristics are denoted as distinct extrusion types in the following. Both processes produce sound wires but are clearly

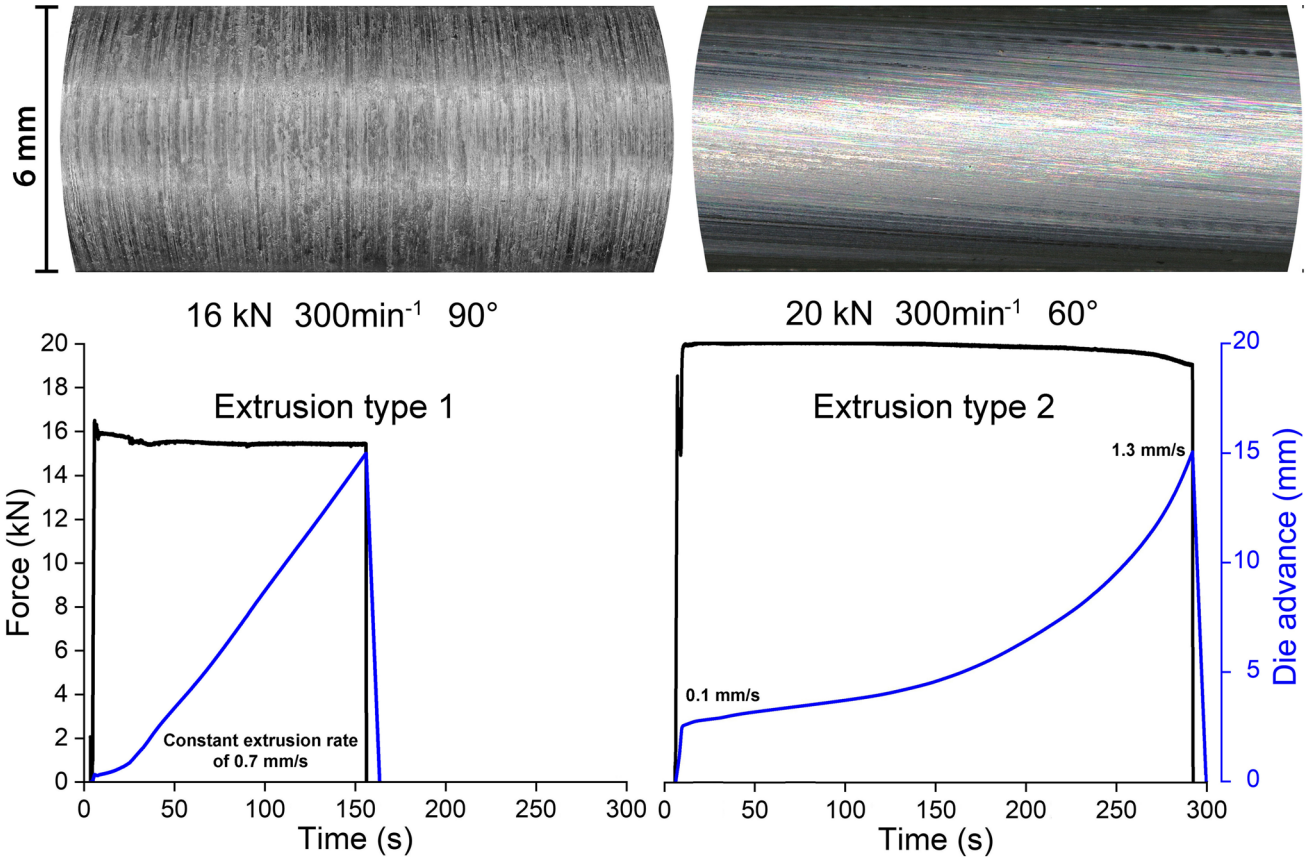

Fig. 9 Different types of process characteristic encountered in FE, showing differences in the surface appearance. FE with 16 kN, 90° die angle, illustrates extrusion type 1, characterized by constant extrusion rate. For FE with 20 kN, 60° die angle, an increasing extrusion rate over time is observed, characterizing extrusion type 2

distinguishable in terms of extrusion rate progression and surface appearance. Extrusion type 1, as presented in the previous section, shows a surface with circumferential, periodic grooves. In contrast, for extrusion type 2 the wire presents a smooth, uniform surface with slightly twisted tooling marks along its length. Hosseini et al. [20] encountered similar surface condition to extrusion type 2 in FE of AA2025-T8 chips, however no correlation between surface condition and final microstructure had been established. To further interpret the observed surface appearance, the theoretical wire length per die rotation is calculated for the position 50 mm from the wire tip, representative for the sections shown in Fig. 9. At this position, the average extrusion rate is 0.7 mm/s in both processes. Considering the applied die rotation of 300 min^{-1}, the introduced rotation amounts to a theoretical extrusion length per die rotation of 0.14 mm. Looking at the resulting surface grooves of extrusion type 1, which are assumed to represent die marks from the relative rotation, 0.15 mm wire length per die rotation is determined by counting periodical surface features per wire length. The observed relative rotation for type 1 extrusions is close to the theoretical value. This implies a mechanically rigid connection between wire and charge material while the applied rotation is converted in sliding friction condition between die and perimeter of the wire. The dependency of this surface macro-roughness on processing parameters has also been reported by Baffari et al. [43]. In contrast, extrusion type 2 leads to a vastly different observation. Calculating the wire length per die rotation from the angle of the surface marks yields approximately 220 mm wire length per die rotation. Due to the continuously increasing extrusion rate over process time for extrusion type 2, this value is only representative for the local conditions in the center of the displayed wire section. However, this result indicates a remarkably low slippage between the forming wire and die, supporting the hypothesis that the relative motion is not converted via sliding friction as in extrusion type 1, but in near sticking friction condition. As a consequence, the applied rotation affects a much larger volume of charge material, leading to a highly effective shear introduction. The subsequent recrystallization in the core of the charge material provides the refined microstructure seen in the wires of extrusion type 2, see microstructure for 20 kN in Fig. 10.

Table 2 Process parameter combination (extrusion force and die angle) studied and observed extrusion type

	16 kN	18 kN	18.5 kN	19 kN	19.5 kN	20 kN	22 kN
90°	1	1				1	
60°	1	1	1	1 and 2	1 and 2	2	2
45°	1						

Note: The 45° die angle led to extrusion rates that exceeded reliable velocity ranges for the used machine setup. Therefore, the effect of higher extrusion forces was not investigated with this die angle

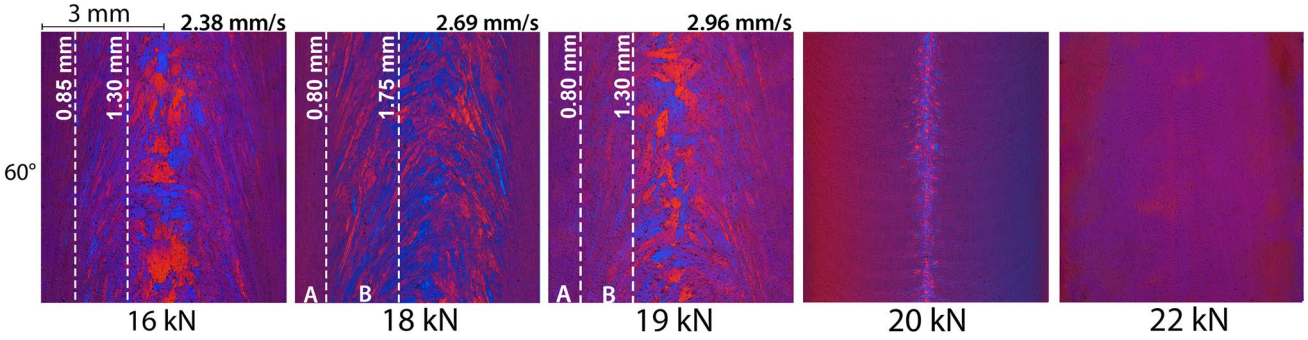

Fig. 10 Resulting wire microstructures for different extrusion forces (16 to 22 kN) using a 60° die angle at 300 min^{-1}. The change in extrusion behavior from type 1 (extrusion rates denoted) to type 2 occurs above 19 kN

As mentioned above, the extrusion rates of the two extrusion types show characteristic differences. For extrusion type 1 a nearly linear (steady-state) increase in die advance is observed, i.e. a constant extrusion rate, while extrusion type 2 starts with an initial jump in the die advance followed by a slow but continuous increase in extrusion rate. It can be seen that for extrusion type 2 the actual extrusion force decreases towards the end of the extrusion, leading to a lower actual force than the set force by the machine, corresponding to the observations made in extrusion type 1 for the full process duration. This difference between the set and actual force during FE can be addressed to the force control setting of the used machine and is a result of the die advance rate exceeding a certain velocity.

By analyzing the process characteristics and surfaces of all studied process combinations, Table 2, it was observed that low extrusion forces and high die angles resulted in steady extrusion rates (extrusions type 1), while high extrusion forces and low die angles resulted in increasing extrusion rates (extrusions type 2). Table 2 summarizes the identified extrusion types found for each parameter combination studied. In the following, the effect of the characteristics of the different extrusion types as well as possible transitions within the process and its implication on the resulting microstructure evolution are discussed more in depth on the basis of the 60° die angle.

The resulting final wire microstructures for different extrusion forces are shown in Fig. 10. As observed already for the 90° die angle, an increase in extrusion force leads first to an increase in size of regions A and B towards the center of the wires. However, above 19 kN extrusion force, there is a drastic change in extrusion behavior from type 1 to type 2, resulting in larger recrystallized volumes in the wire, see Fig. 10. For an extrusion force of 22 kN, a completely recrystallized wire was observed, i.e. effectively eliminating the Region C. Therefore, this wire is further characterized, see Fig. 11. For a measured region in the center of the extruded wire at 22 kN, an average grain size of 1.2 µm and a high fraction of high-angle grain boundaries, around 83.8 %, was determined via EBSD, showing clearly the strong refinement of the microstructure compared to the initial charge material.

A transition from extrusion type 1 to type 2 was not observed for the 90° die angle, which can probably be attributed to the different initial material flow conditions for the lower die angles in the first stages of extrusion, see Fig. 8. The material flow associated with the 60° die angle possibly provides increased flow resistance, whether related to turbulence or effectively lower temperatures. This allows for higher applied axial forces to not directly result in an increased extrusion rate but rather higher contact pressure at the die-charge interface. This enables the observed sticking friction conditions to establish, Fig. 9, and leads to conversion of the applied rotation in shearing over a large volume of affected charge material. In this aspect, the die angle assists in directing the imposed deformation towards the center of the charge material. The charge material affected by this shearing provides the fully recrystallized structure

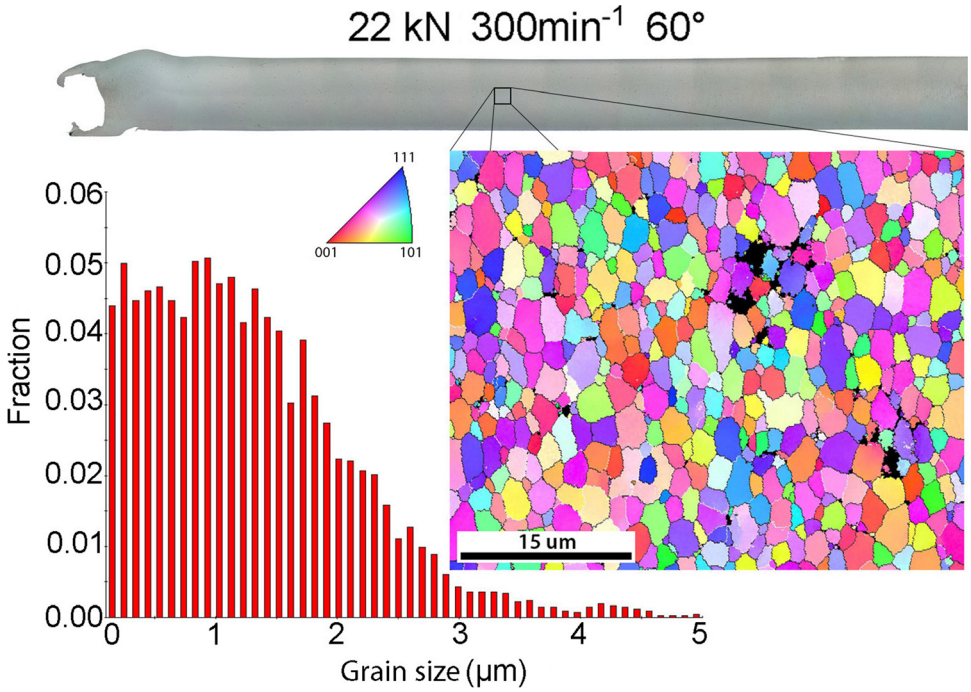

Fig. 11 Microstructure and grain size distribution of a wire extruded with 22 kN, 60° die angle at 300 min^{-1}. 81% of the grains are smaller than 2 µm and 42% are within submicrometer range

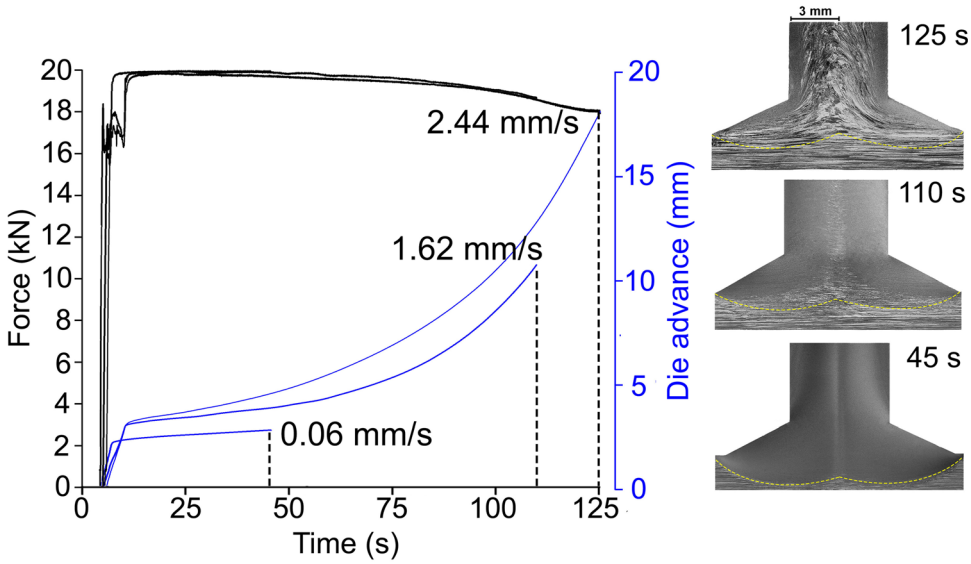

Fig. 12 Process and microstructural evolution in FE using 20 kN extrusion force, 60° die angle at 300 min^{-1}. The microstructural evolution from type 2 to the typical microstructure expected for extrusion type 1 can be seen. Both the microstructure of the charge material as well as in the wire change as the extrusion progresses

present in the wires extruded with 60° tool at forces at approximately 20 kN, Fig. 10.

Since extrusion type 2 is characterized by a continuously increasing extrusion rate, i.e. a non-steady-state extrusion behavior, the microstructure evolution is analyzed via serial extrusions at different stages of the extrusion process. For this purpose, extrusions at 20 kN extrusion force are analyzed in detail, Fig. 12[3]. The initial phase (45 s) of the process is characterized by a low extrusion rate, which is associated with a general high portion of recrystallization in the charge material in front of the die and in the wire. In the intermediate stage (110 s), a reduction of the recrystallized volume is present, associated with a simultaneous increase in extrusion rate. In the

[3] Although the extrusions are performed at the same process parameters and conditions, slight variations within the extrusion process can be seen in the extrusion force and die advance curves for the different processes in Fig. 12.

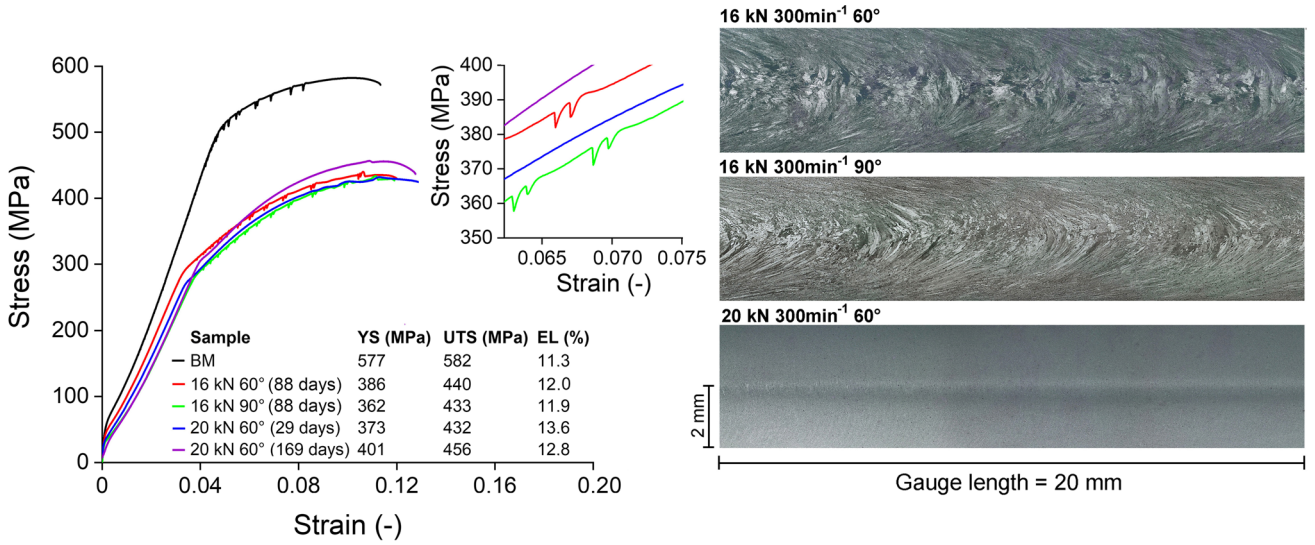

Fig. 13 Tensile test results and microstructure of the extruded wires. Extruded wires show lower strength and higher elongation at break than base material. The fully recrystallized wires (20 kN, 300 min^{-1}, 60°) show the highest ductility, 20 % higher than the base material, and suppression of the PLC effect

last stage (125 s), both the microstructure as well as the extrusion rate reach conditions typical for extrusion type 1, see for instance Fig. 8. During the extrusion process, the measured temperature elevates and larger volumes of material can be plasticized. This reduction in extrusion resistance allows the extrusion rate to increase, leading to a reduction in recrystallized volume due to the shorter exposure of the charge material to the applied shearing. At the same time, the higher temperature increases the shear gradient reaching from the die-charge interface into the charge material, reducing subsequently the depth and volume of sufficiently recrystallized charge material. The microstructure at later process stages reveals this shift of shearing from the charge material towards the die face, see Fig. 12. This shift ultimately leads to conversion of a large amount of the imposed rotation at the die-charge interface, respectively sliding friction in this zone.

Following the presented hypothesis, extrusion type 2 is associated with the shear introduction over a larger volume, effectively leading to complete recrystallization of the extruded material. This condition is affected by the combination of low die angles, higher extrusion forces and initial material flow, leading to sticking friction at the die-charge interface. However, this condition changes as the extrusion progresses and processing temperature increases, deteriorating shear and material flow conditions.

In the next section, the effect of the different resulting microstructures on the mechanical properties is discussed.

Mechanical properties of extruded wires

Since the tensile testing specimens needed to be machined from the extruded wires, the outer refined layer (Region A) was effectively removed from the type 1 extruded wires, leaving only regions B and C. Besides the base material, specimens from three different extrusion parameters were tested, including two different sets of wires for extrusion type 1 (16 kN, 300 min^{-1}, 90° and 16 kN, 300 min^{-1}, 60°) and one set for extrusion type 2 (20 kN, 300 min^{-1}, 60°), i.e. partially and fully recrystallized wire material. The resulting stress-strain curves, as well as the microstructure of the tested specimens, are illustrated in Fig. 13.

The results show a lower strength and slightly higher elongation at break for the extruded wires in comparison to the base material. The fully recrystallized wires (20 kN, 300 min^{-1}, 60°) show the highest ductility, around 20 % higher than the base material. It is noteworthy that the AA7075 base material used had previously received thermal and mechanical processing (T651), in specific precipitation hardening heat treatment and mechanical processing by rolling [26], which provided high initial mechanical properties. For the present temperatures during FE, Fig. 6, precipitates may dissolve or coarsen [44–46], i.e. affecting the present precipitation hardening, resulting in yield and ultimate tensile strength in typical ranges for AA7075 after annealing heat treatment [45]. The average hardness of a wire of extrusion type 1 (16 kN, 300 min^{-1}, 90° die angle), tested 65 days after extrusion, was determined as 128 ± 7 HV, while the hardness results did

not reveal any correlation to the level of refinement in the regions formed. Due to the initial T651 condition, the base material showed a higher hardness of 180 HV. The hardness results of the extruded wires agree with the FSW/P literature on AA7075-T651, where Fuller et al. [44] determined the hardness in the TMAZ in range of 115 to 130 HV after 49 days of natural aging.

The effect of natural aging was observed on completely refined wires extruded at 20 kN, 300 min^{-1}, 60°, see Fig. 13. A minimal reduction in elongation at break but a slight increase in yield and ultimate tensile strength was observed for the additional aging time of 140 days.

It is interesting to note that the Portevin-Le Chatelier (PLC) effect, characterized by stress serration patterns in the stress-strain curve, is seen for most of the samples, except for the completely recrystallized wires, Fig. 13. In this wire material, the PLC effect remains suppressed even after longer periods of natural aging. The PLC effect leads to plastic instabilities caused by Mg atoms locking dislocations and working against their movements in AlMg alloys [47]. Since the PLC effect is influenced by grain size [48] and its mechanism is associated with solute atom-dislocation interactions [49–51], as well as with the different types of precipitates present in the alloy [52], the suppression of the PLC in the stress-strain behavior can be explained by microstructural modifications promoted by extrusion type 2. This suppression might be induced not only by the resulting grain refinement, but also by possible solute-atom (Mg) or precipitates related effects. In the literature, Lebedkina et al. [53] reported that severe plastic deformation may effectively suppress the macroscopic stress serrations characteristic of the PLC effect in AlMg alloys. The present findings on the extruded wires suggest a possible existence of similar effects on the resulting mechanical behavior of AlMgZn metallic systems processed by severe plastic deformation.

Conclusion

In summary, this study reveals two different extrusion types during friction extrusion of AA7075-T651, showing different process characteristics, surface appearances and microstructures. The main findings can be summarized as follows:

- Two distinct conditions in FE were analyzed: one related to low extrusion forces and high die angles that leads to a constant extrusion rate but providing only partially refined wires; a second one related to high extrusion forces and low die angles, capable of fully recrystallizing the microstructure of the extruded wires but presenting continuous increase in extrusion rate during the process.
- The microstructural refinement originates in the charge material. The more effective the shear introduction from the die into the charge, the greater the amount of recrystallized wire material.
- Sound wires at an extrusion ratio of 6.25 were produced, showing for the fully recrystallized wire an average grain size of 1.2 µm, with 42 % of ultra-refined grains, i.e. smaller than 1 µm. As a result, these wires presented an increase in elongation at break of around 20 % compared to the base material.
- Die angle, material flow and friction conditions in the initial stages of the FE process as well as thermal condition throughout processing are decisive for the microstructural homogeneity and refinement in the extruded wire material.

Funding Open Access funding enabled and organized by Projekt DEAL. B. Klusemann acknowledges funding from the European Research Council (ERC) under the European Union's Horizon 2020 research and innovation programme (grant agreement No 101001567).

Data availability The data related to this research is available online (https://doi.org/10.5281/zenodo.5910351).

Declarations

Conflicts of interest The authors declare that they have no conflict of interest.

References

1. Huang Y, Langdon TG (2013) Advances in ultrafine-grained materials. Materials Today 16(3):85–93. https://doi.org/10.1016/j.mattod.2013.03.004
2. Alvandi H, Farmanesh K (2015) Microstructural and mechanical properties of nano/-fine structured 7075 aluminum alloy by accumulative roll-bonding process. Procedia Materials Science 11:17–23. https://doi.org/10.1016/j.mspro.2015.11.020
3. Das, S.K., Yin, W.: The worldwide aluminum economy: The current state of the industry. Jom 59(11), 57–63 Springer (2007) https://doi.org/10.1007/s11837-007-0142-0
4. Magalhães VM, Leitão C, Rodrigues DM (2018) Friction stir welding industrialisation and research status. Science and Technology of Welding and Joining 23(5):400–409. https://doi.org/10.1080/13621718.2017.1403110

5. Wang G, Zhao Y, Hao Y (2018) Friction stir welding of high-strength aerospace aluminum alloy and application in rocket tank manufacturing. Journal of Materials Science & Technology 34(1):73–91. https://doi.org/10.1016/j.jmst.2017.11.041
6. Hattingh DG, von Wielligh L, Thomas W, James MN (2015) Friction processing as an alternative joining technology for the nuclear industry. Journal of the Southern African Institute of Mining and Metallurgy 115:903–912. https://doi.org/10.17159/2411-9717/2015/v115n10a2
7. Martin J, Wei S (2015) Friction stir welding technology for marine applications. In: Friction stir welding and processing VIII, pp 219–226. Springer, Wallis Way, Catcliffe, Rotherham, S60 5TZ, UK. https://doi.org/10.1007/978-3-319-48173-9_24
8. Thomas W, Nicholas E, Kallee S (2001) Friction based technologies for joining and processing. In: Paper presented at TMS friction stir welding and processing conference, November 2001, Indianapolis
9. Haghshenas M, Gerlich AP (2018) Joining of automotive sheet materials by friction-based welding methods: A review. Engineering Science and Technology, an International Journal 21(1):130–148. https://doi.org/10.1016/j.jestch.2018.02.008
10. Ansari MA, Behnagh RA, Narvan M, Naeini ES, Givi MKB, Ding H (2016) Optimization of friction stir extrusion (FSE) parameters through taguchi technique. Transactions of the Indian Institute of Metals 69(7):1351–1357. https://doi.org/10.1007/s12666-015-0686-6
11. Tang W, Reynolds AP (2010) Production of wire via friction extrusion of aluminum alloy machining chips. Journal of Materials Processing Technology 210(15):2231–2237. https://doi.org/10.1016/j.jmatprotec.2010.08.010
12. Thomas WM, Nicholas ED, Needham JC, Much MG, Temple-smith P, Dawes CJ (1991) Friction stir welding. Patent Application N° 9125978.8
13. Li X, Tang W, Reynolds AP, Tayon WA, Brice CA (2016) Strain and texture in friction extrusion of aluminum wire. Journal of Materials Processing Technology 229:191–198. https://doi.org/10.1016/j.jmatprotec.2015.09.012
14. Tahmasbi K, Mahmoodi M (2018) Evaluation of microstructure and mechanical properties of aluminum A7022 produced by friction stir extrusion. Journal of Manufacturing Processes 32:151–159. https://doi.org/10.1016/j.jmapro.2018.02.008
15. Weglowski MS, Dymek S, Hamilton C (2013) Experimental investigation and modelling of friction stir processing of cast aluminium alloy AlSi9Mg. Bulletin of the Polish Academy of Sciences. Technical Sciences 61(4):93–904
16. Whalen S, Joshi V, Overman N, Caldwell D, Lavender C, Skszek T (2017) Scaled-up fabrication of thin-walled ZK60 tubing using shear assisted processing and extrusion. In: Solanki KN, Orlov D, Singh A, Neelameggham NR (eds.) Magnesium Technology 2017, pp 315–321. Springer, Cham. https://doi.org/10.1007/978-3-319-52392-7_45
17. Guo J (2015) Solid state welding processes in manufacturing. In: Nee AYC, Handbook of manufacturing engineering and technology, pp 569–592. Springer London, London. https://doi.org/10.1007/978-1-4471-4670-4_554
18. Black JT, Kohser RA (2019) DeGarmo's materials and processes in manufacturing. 13 edn. John Wiley & Sons, 111 River Street, Hoboken, NJ 07030-5774, USA
19. Ghosh A (2001) Segregation in cast products. Sadhana 26:5–24. https://doi.org/10.1007/BF02728476
20. Hosseini A, Azarsa E, Davoodi B, Ardahani Y (2012) Effect of process parameters on the physical properties of wires produced by friction extrusion method. International Journal of Advances in Engineering & Technology 3(1):592 Citeseer
21. Behnagh RA, Mahdavinejad R, Yavari A, Abdollahi M, Narvan M (2014) Production of wire from AA7277 aluminum chips via friction-stir extrusion (FSE). Springer, pp 1484–1489
22. Cepeda-Jiménez CM, García-Infanta JM, Ruano OA, Carreño F (2011) Mechanical properties at room temperature of an al-zn-mg-cu alloy processed by equal channel angular pressing. Journal of Alloys and Compounds 509(35):8649–8656. https://doi.org/10.1016/j.jallcom.2011.06.070
23. Jayaganthan R, Brokmeier H-G, Schwebke B, Panigrahi SK (2010) Microstructure and texture evolution in cryorolled al 7075 alloy. Journal of Alloys and Compounds 496(1):183–188. https://doi.org/10.1016/j.jallcom.2010.02.111
24. Gerlich A, Yamamoto M, North T (2007) Local melting and cracking in al 7075–t6 and al 2024–t3 friction stir spot welds. Science and Technology of Welding and Joining 12:472–480. https://doi.org/10.1179/174329307X213873
25. Whalen S, Olszta M, Reza-E-Rabby M, Roosendaal T, Wang T, Herling D, Taysom BS, Suffield S, Overman N (2021) High speed manufacturing of aluminum alloy 7075 tubing by shear assisted processing and extrusion (ShAPE). Journal of Manufacturing Processes 71:699–710. https://doi.org/10.1016/j.jmapro.2021.10.003
26. Smallman RE, Bishop RJ (1999) Modern physical metallurgy and materials engineering, 6th edn. Butterworth-Heinemann, Oxford, United Kingdom
27. Zhang H, Zhao X, Deng X, Sutton MA, Reynolds AP, McNeill SR, Ke X (2014) Investigation of material flow during friction extrusion process. International Journal of Mechanical Sciences 85:130–141. https://doi.org/10.1016/j.ijmecsci.2014.05.011
28. Li X, Tang W, Reynolds A (2013) Material flow and texture in friction extruded wire. In: Friction stir welding and processing VII, pp 339–347. Springer, USA. https://doi.org/10.1007/978-3-319-48108-1_35
29. Li X, Reza-E-Rabby M, Ryan M, Grant G, Reynolds A (2021) Evaluation of orthogonal strain components in friction extrusion. Journal of Materials Research and Technology 15, 3357–3364 Elsevier. https://doi.org/10.1016/j.jmrt.2021.10.001
30. Kayser T, Klusemann B, Lambers H, Maier H, Svendsen B (2010) Characterization of grain microstructure development in the aluminum alloy EN AW-6060 during extrusion. Materials Science and Engineering: A 527(24–25):6568–6573. https://doi.org/10.1016/j.msea.2010.06.050
31. Saha P (2000) Aluminum extrusion technology. ASM International, Ohio 44073-0002, USA
32. Baffari D, Reynolds AP, Li X, Fratini L (2017) Influence of processing parameters and initial temper on friction stir extrusion of 2050 aluminum alloy. Journal of Manufacturing Processes 28:319–325. https://doi.org/10.1016/j.jmapro.2017.06.013
33. Behnagh RA, Shen N, Ansari MA, Narvan M, Besharati Givi MK, Ding H (2016) Experimental analysis and microstructure modeling of friction stir extrusion of magnesium chips. Journal of Manufacturing Science and Engineering 138(4) https://doi.org/10.1115/1.4031281
34. Rajamuthamilselvan M, Ramanathan S (2011) Hot deformation behaviour of 7075 alloy. Journal of Alloys and Compounds 509(3):948–952. https://doi.org/10.1016/j.jallcom.2010.09.139
35. Kaibyshev R, Malopheyev S (2014) Mechanisms of dynamic recrystallization in aluminum alloys. In: Marthinsen K, Holmedal B, Li Y (eds.) Aluminium Alloys 2014 - ICAA14, vol 794, pp 784–789. Trans Tech Publications Ltd, Switzerland. https://doi.org/10.4028/www.scientific.net/MSF.794-796.784
36. Dieter G, Kuhn H, Semiatin SL (2003) Handbook of workability and process design hardcover, p 400. ASM International, Ohio, USA
37. Ravichandran N, Prasad Y (1991) Dynamic recrystallization during hot deformation of aluminum: a study using processing maps.

Metallurgical Transactions A 22(10), 2339–2348 Springer, https://doi.org/10.1007/BF02665000
38. Alaneme KK, Okotete EA (2019) Recrystallization mechanisms and microstructure development in emerging metallic materials: A review. Journal of Science: Advanced Materials and Devices 4(1):19–33. https://doi.org/10.1016/j.jsamd.2018.12.007
39. Shojaei K, Sajadifar SV, Yapici GG (2016) On the mechanical behavior of cold deformed aluminum 7075 alloy at elevated temperatures. Materials Science and Engineering: A 670:81–89. https://doi.org/10.1016/j.msea.2016.05.113
40. Totten GE, MacKenzie DS (2003) Handbook of aluminum: alloy production and materials manufacturing. 2, 1st edn. CRC press, Boca Raton. https://doi.org/10.1201/9780203912607
41. Yu H, Park SH, You BS (2015) Die angle dependency of microstructural inhomogeneity in an indirect-extruded AZ31 magnesium alloy. Journal of Materials Processing Technology 224:181–188. https://doi.org/10.1016/j.jmatprotec.2015.05.003
42. Rios PR, Siciliano F Jr, Sandim HRZ, Plaut RL, Padilha AF (2005) Nucleation and growth during recrystallization. Materials Research 8(3):225–238. https://doi.org/10.1590/S1516-14392005000300002
43. Baffari D, Buffa G, Campanella D, Fratini L, Reynolds AP (2017) Process mechanics in friction stir extrusion of magnesium alloys chips through experiments and numerical simulation. Journal of Manufacturing Processes 29:41–49. https://doi.org/10.1016/j.jmapro.2017.07.010
44. Fuller CB, Mahoney MW, Calabrese M, Micona L (2010) Evolution of microstructure and mechanical properties in naturally aged 7050 and 7075 Al friction stir welds. Materials Science and Engineering: A 527(9):2233–2240. https://doi.org/10.1016/j.msea.2009.11.057
45. Isadare AD, Aremo B, Adeoye MO, Olawale OJ, Shittu MD (2013) Effect of heat treatment on some mechanical properties of 7075 aluminium alloy. Materials Research 16(1):190–194. https://doi.org/10.1590/S1516-14392012005000167
46. Souza SHD, Padilha AF, Kliauga AM (2019) Softening behavior during annealing of overaged and cold-rolled aluminum alloy 7075. Materials Research 22. https://doi.org/10.1590/1980-5373-MR-2018-0666
47. Moradpour M, Khodabakhshi F, Eskandari H (2019) Dynamic strain aging behavior of an ultra-fine grained Al-Mg alloy (AA5052) processed via classical constrained groove pressing. Journal of Materials Research and Technology 8(1):630–643. https://doi.org/10.1016/j.jmrt.2018.04.016
48. Yuzbekova D, Mogucheva A, Zhemchuzhnikova D, Lebedkina T, Lebyodkin M, Kaibyshev R (2017) Effect of microstructure on continuous propagation of the Portevin-Le Chatelier deformation bands. International Journal of Plasticity 96:210–226. https://doi.org/10.1016/j.ijplas.2017.05.004
49. Tian N, Wang G, Zhou Y, Liu K, Zhao G, Zuo L (2018) Study of the portevin-le chatelier (PLC) characteristics of a 5083 aluminum alloy sheet in two heat treatment states. Materials. https://doi.org/10.3390/ma11091533
50. Zhemchuzhnikova D, Lebyodkin M, Yuzbekova D, Lebedkina T, Mogucheva A, Kaibyshev R (2018) Interrelation between the Portevin-Le Chatelier effect and necking in AlMg alloys. International Journal of Plasticity 110:95–109. https://doi.org/10.1016/j.ijplas.2018.06.012
51. Zhemchuzhnikova D, Lebyodkin MA, Lebedkina TA, Kaibyshev RO (2015) Unusual behavior of the Portevin-Le Chatelier effect in an AlMg alloy containing precipitates. Materials Science and Engineering: A 639:37–41. https://doi.org/10.1016/j.msea.2015.04.094
52. Chen J-Z, Zhen L, Fan L-W, Yang S-J, Dai S-L, Shao W-Z (2009) Portevin-Le Chatelier effect in Al-Zn-Mg-Cu-Zr aluminum alloy. Transactions of Nonferrous Metals Society of China 19(5):1071–1075. https://doi.org/10.1016/S1003-6326(08)60408-2
53. Lebedkina TA, Lebyodkin MA, Lamark TT, Janeček M, Estrin Y (2014) Effect of equal channel angular pressing on the Portevin-Le Chatelier effect in an Al3Mg alloy. Materials Science and Engineering: A 615:7–13. https://doi.org/10.1016/j.msea.2014.07.064